CHEMICAL SCIENCES

TiO$_2$ nanotubes decorated with Au nanoparticles for Photocatalytic Hydrogen Generation under UV-Visible and Visible Light Irradiations

JEAN CLAUDIO S. COSTA, NOELIA FRANCO, THIAGO ANDRÉ S. SOARES,
NAYTHALLA ANGELA M. SARAIVA, MARCO AURÉLIO S. GARCIA,
JOHAN RENE GONZALEZ & GIOVANNA MACHADO

Abstract: The development of stable and active TiO$_2$ nanotubes (NTs) decorated with plasmonic gold nanoparticles (Au NPs) represents a strategy for charge-transfer processes improvements. However, organic capping ligands used for Au NPs synthesis usually remain on the surface of the metal, leading to poor Schottky junctions between Au and TiO$_2$. Herein, we report on the synthesis of a nanotubular matrix of TiO$_2$ decorated with gold without the need of ligands. The Au NPs mean diameter (12 nm) was similar to all the samples prepared, no matter the metal loading. Such materials enabled to use the metal as a cocatalyst for photogeneration of H$_2$ under UV and visible light irradiations. We found an optimum metal loading (2.6 wt% Au) that enabled an improvement of 760% on the H$_2$ production when compared to the bare TiO$_2$ NTs under UV-Vis irradiation. In addition, such catalyst was able to perform photogeneration of H$_2$ under visible irradiation, which was not conceivable before the metal immobilization over the TiO$_2$ NTs. The yield obtained was comparable to the observed when the catalyst was used under UV-Vis conditions. The produced materials were fully characterized by UV-Vis, XRD, TEM, and SEM.

Key words: Nanotubular TiO$_2$, Gold nanoparticles, Photogeneration of H$_2$, UV and visible light.

INTRODUCTION

The world demand for fossil fuels has been increasing year-to-year since most of the global energy consumption is directly related to petroleum-derived products (Young et al. 2017). Nevertheless, due to the instability of oil sources and price augmentation, there is a real long-term energy crisis developing over the years (Zhang et al. 2017). In addition to the fuel shortage, the production, transportation, storage and use of this energetic matrix have adverse effects on the environment. Accordingly, the need for using renewable energy sources without (or fewer) impacts on the climate is genuinely better in all senses and, among some options currently available, sunlight energy must be highlighted as 885 million TWh of its power reaches the Earth's surface in a year (Bessarabov et al. 2016).

Within this scenario, hydrogen is an attractive alternative energy source and there is a great interest in the development of sustainable and cheap methods for its production. Since the first report on the water splitting on TiO$_2$ electrode, this photoelectrochemical process has become a promising way to produce hydrogen by using solar energy (Fujishima & Honda 1972). However, the efficiency of TiO$_2$ for water splitting may be considered somehow limited due to the high

recombination rate of photogenerated electron-hole pairs (Ni et al. 2007) and limited utilization of visible light. In an attempt to overcome these issues, nanotubular materials have been proposed to replace disordered materials targeting charge transport improvements (Cho et al. 2015). Noble metal cocatalysts (Bamwenda et al. 1995, Gomes Silva et al. 2011) have been immobilized on highly structured TiO$_2$ materials to enhance their activity by narrowing their band gap to absorb visible light (Hoffmann et al. 1995). Well-dispersed Au NPs act as cocatalysts when impregnated on TiO$_2$ NTs and several reports demonstrated optimized efficiency for H$_2$ production. The reasons for this synergetic effect is the strong absorption ability of Au NPs, which present surface plasmon resonance (SPR) that improves the response of visible light. The fast electron transfer from TiO$_2$ to Au NPs traps the photogenerated electrons and prevent their recombination with holes (Lee et al. 2013, Gao et al. 2014). Working on this aspect, Reichert et al. (2015), have also demonstrated that the photocatalytic H$_2$ evolution depends strongly on the Au loading on TiO$_2$ catalyst film electrodes and Rayalu et al. 2013, proved that the catalyst synthesis pathway highly influences the hydrogen generation.

Considerable efforts have been doing in the development of more efficient catalysts for water splitting reactions; however, organic capping ligands used for Au NPs (Millstone et al. 2009, Rycenga et al. 2011) synthesis remain in the interface of the metal and the NTs, leading to poor Schottky junctions between Au and TiO$_2$. The possibility of removal of these ligands by calcination (Liu & Aydil 2009), chemical oxidation (Liu et al. 2013), and solvent extraction (Lopez-Sanchez et al. 2011) are limited, due to the modification of the nanostructures morphology, which may affect the resonance properties or their efficiency. Therefore, it is extremely desired

to develop methods without organic moieties in the interface.

Previously, we reported a method for the growth of TiO$_2$ films arrays with simultaneous metal nanoparticle impregnation during anodic oxidation, which enabled the photogeneration of H$_2$. However, we used supported nanotubes and only one face was used for photogeneration (Feil et al. 2010).

Herein, we report on the synthesis of decorated with Au as a cocatalyst for photogeneration of H$_2$, without the need of organic capping ligands or bifunctional linker molecule (Kongkanand et al. 2008). In addition, isoladots TiO$_2$ NTs was prepared, from the film using H$_2$O$_2$ searching for enabling greater photogeneration.

We evaluated how the metal loading may affect photocatalytic H$_2$ evolution on isolated TiO$_2$ NTs and how their amount may influence Raman peaks shifts and enlargements for three Au metal loading samples. UV-Vis, XRD, TEM and SEM analyses were also performed to shed some light on the catalyst role.

EXPERIMENTAL SECTION

All chemicals used in the experiments were of analytical grade, bought from Sigma-Aldrich, and used without further purification.

Preparation of TiO$_2$ NTS

Titanium foils (0.10 mm thick, 98.6%, Realum) were used for the processes herein performed. TiO$_2$ NTs were prepared by electrochemical anodization of the metallic foils, which were polished with sandpaper, cleaned in an ultrasound cleaner (with a solution of water, acetone and 10 wt% extran) for 10 min, washed with water and ethanol, rinsed with ultrapure water and dried under N$_2$ flow. Electrochemical

anodization was performed in an ethylene glycol (EG) solution containing 10 wt% H$_2$O and 0.25 wt% NH$_4$F at 30 V for 30 min. A cathode/anode ratio of 1:1 was maintained for the anodization processes with an anodization voltage ramp of 5 V. s^{-1} at room temperature. In order to crystallize the TiO$_2$ NTs, the samples were calcined in a furnace with air flow in a heating rate of 10 °C min^{-1}, from room temperature to 400 °C, which was maintained for 3 h. Then, the foils were anodized again, in order to release the NTs. The process was identical to the described before, but it was performed for 10 min instead of 30 min. After such procedure, the foils were washed with H$_2$O$_2$ to collect the isoladots NTs. Such solution was centrifuged and the NTs were washed several times with water before storage in an amber bottle.

Cocatalyst Immobilization

In a typical procedure, 10 mg of TiO$_2$ NTs were added under vigorous stirring in an aqueous solution of 1 wt% ascorbic acid. Then, 80, 150 or 220 µL of an aqueous solution of 1% AuCl$_{4(aq)}$ (m/m) were added and the mixture was heated to 110 °C and kept under stirring for 2 h. Such processes allowed the preparation of catalysts with 1.8 (80 µL), 2.6 (150 µL) and 3.7 wt% Au (220 µL). After the Au NPs immobilization, the materials were designated as TiO$_2$Au and its Au wt% content is specified throughout the text, when necessary.

Nanotubes Characterization

Transmission electron microscopy (TEM) images were obtained using a Tecnai G2 microscope (Massachusetts, EUA, Thermo Fisher Scientific) operating at 200 kV, and scanning electron microscopy (SEM) images were obtained using a Quanta 200 FEG operating at 20kV. The samples for TEM images were prepared by drop casting an isopropanol suspension of the samples over

a carbon-coated copper grid, followed by drying under ambient conditions. The samples for SEM images were prepared by drop-casting an aqueous suspension of the nanostructures over a Si wafer, followed by drying under ambient conditions. The X-ray diffractograms were obtained using a Bruker ADVANCE 8 equipment with monochromatic CuKα radiation (λ = 1.54056 Å) and a graphite monochromator. The voltage of the copper emission tube was 40 kV and the filament current was 40 mA, at a 2θ range from 20º to 80° with a 0.02° step size and measuring time of 5s per step. The metal content in all catalysts was measured by FAAS with a Shimadzu AA-6300 atomic absorption spectrophotometer. The instrumental parameters and experimental conditions used for Au measurement were: wavelength = 242.8 nm; lamp current = 5 mA; bandpass = 0.7 nm; height of observation = 7 mm; air flow rate = 15 L min^{-1}; acetylene flow rate = 2.0 L min^{-1}; reading time = 5 s; nebulizer aspiration flow rate = 4 mL min^{-1}. The Raman spectra were recorded using a Scanning Near-field Optical Microscope (SNOM) Alpha 300 S Witec equipment. The samples were irradiated with the 532 nm line laser. The UV-Vis and reflectance analyses were performed in a Cary 300 UV-Vis Agilent equipment.

Photocatalytic Hydrogen Generation

Hydrogen photogeneration experiments were carried out in a calibrated 35-mL gas-enclosed photochemical double quartz reactor in which water circulates and controls the solution temperature (25° C) under continuous magnetic stirring. The catalysts (7.5 mg) were dispersed in 15 mL of a 5 wt% Glycerol aqueous solution and introduced into the reactor (Vaidya & Rodrigues 2009, Schwengber et al. 2016). Prior to irradiation, the system was deaerated using Ar-vacuum cycles for about 10 min to reduce the oxygen content. The photocatalytic activity

of the material was studied for H$_2$ generation by water-splitting reaction under UV-Visible irradiation for 3 hours.

The photoanodes were illuminated by a 600 W solar simulator (Newport, EUA, Power solar) and a 450W Xe lamp (California, EUA, Ushio) at one sun intensity. The light intensity incidence was measured with a calibrated Si photodiode. When necessary, FSQ-GG400 and FSQ-UG5 filters (California, EUA, Newport Corporation) were used to select the radiation wavelength. The amount of accumulated H$_2$ produced in the headspace of sealed quartz reactors was measured using an Agilent gas chromatograph equipped with a TCD detector and HP-PLOT/Q and HPMOLESIEVE columns of 30 m each. For rate determination, data were taken at regular intervals from 30 min to 210 min. A maximum volume of 450 µL of the gas contained in the closed reactor was collected with a gas-tight syringe (Sample Lock Syring, Hamilton).

RESULTS AND DISCUSSION

SEM and TEM images of the resulting TiO$_2$ NTs decorated with Au NPs are shown in Fig. 1. The SEM top view image (Fig. 1a) of the TiO$_2$Au (2.6 wt% Au) material and the size distribution histogram (Supplementary Material – Fig. S1) revealed an average diameter of the NTs of 105 nm. The size distribution was found to be well described by a lognormal function and the narrow size distribution shows the robustness of the described approach for TiO$_2$ NTs synthesis. Fig. 1 also shows TEM images of the TiO$_2$ nanotubes decorated with different Au loadings, i.e., 1.8 wt% (Fig. 1b), 2.6 wt% (Fig. 1c), and 3.7 wt% (Fig. 1d). The syntheses of the three samples were performed using the same reaction conditions, changing
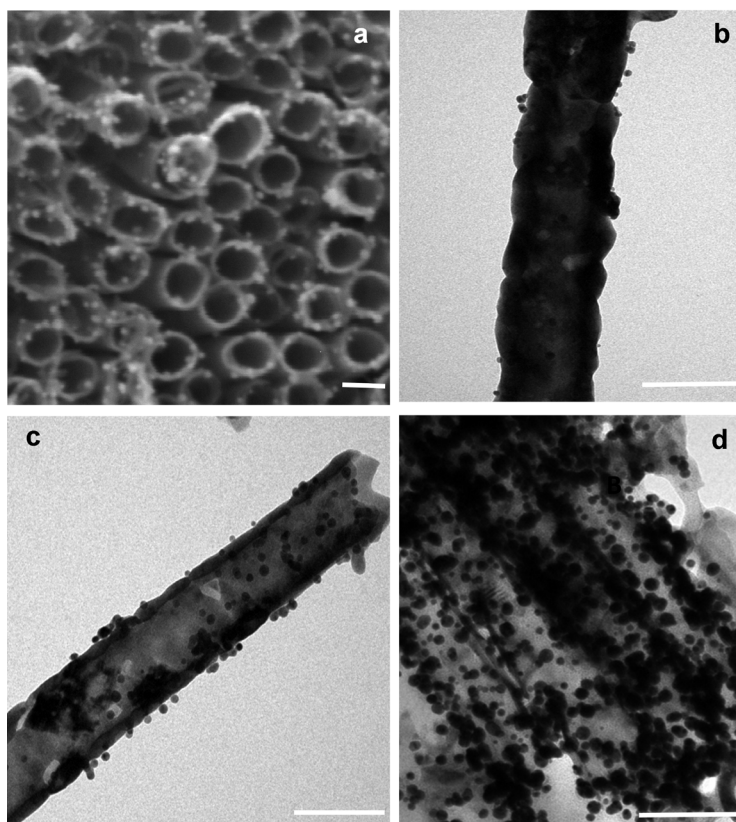

Figure 1. (a) Top view SEM image of TiO$_2$ nanotubes. TEM images of (b) 1.8, (c) 2.6, and (d) 3.7 wt% Au decorating the TiO$_2$ NTs (scale bars of 100 nm).

the Au concentrations during the procedure as stated in the Experimental Section. The mean diameter of the NPs of 12 nm is the same for all the samples, according to the size distribution histograms (Fig. S2); the three samples were found to present NPs homogenously distributed all over the NTs. EDS analysis was performed for the 1.8 wt% Au sample (Fig. S3) and revealed that its composition corresponds to the elements expected (Au, Ti, O), according to the emission lines obtained. Since the catalysts were synthesized using the same approach, the result may be extended to encompass the samples with another metal loading. In addition, the results for the 1.8 wt% Au sample validated the amount of Au loading obtained by using FAAS (1.8 wt% Au), since the EDS technique allowed to calculate a 1.9 wt% Au content.

XRD analysis of the as-prepared TiO$_2$ NTs indicated that anatase crystalline phase was present in the sample since the experimental XRD pattern agrees with the JCPDS card no. 89-4921, as shown in Fig. 2 (red line). The 2θ peaks at 25.3°, 37.8°, 48.0°, 54.6°, 62.7°, 69.5° and 75.0° confirm its anatase crystalline structure.

At the reaction conditions performed, no expressive secondary impurity peaks from other polymorphs of titania, namely the rutile and brookite crystal phases, were present. The obtained XRD diffraction pattern of TiO$_2$Au (2.6 wt% Au) was also studied and is represented by the black line in Fig. 2. The most representative Au XRD peaks occurred at 38.2°, 44.4° and 64.0°, which corresponded to (111), (200) and (220) planes, respectively (JCPDS card no. 04-0784); the results suggested that the Au NPs crystallized in a face-centered cubic (fcc) lattice. Data also showed that essentially the anatase crystal structure was preserved after the TiO$_2$Au catalyst synthesis, which is a very important feature claimed for water splitting reactions. However, as shown in the inset of the enlarged profile between 35.0° and 45.0°, a slight broadening of the anatase peak at 37.8° was observed. Apparently, gold immobilization slightly affected the crystallography of the anatase phase. As seen before (red line) a low-intensity peak was observed in the hydrothermally produced TiO$_2$. After the cocatalyst adding, such peak increased, suggesting peaks overlap between
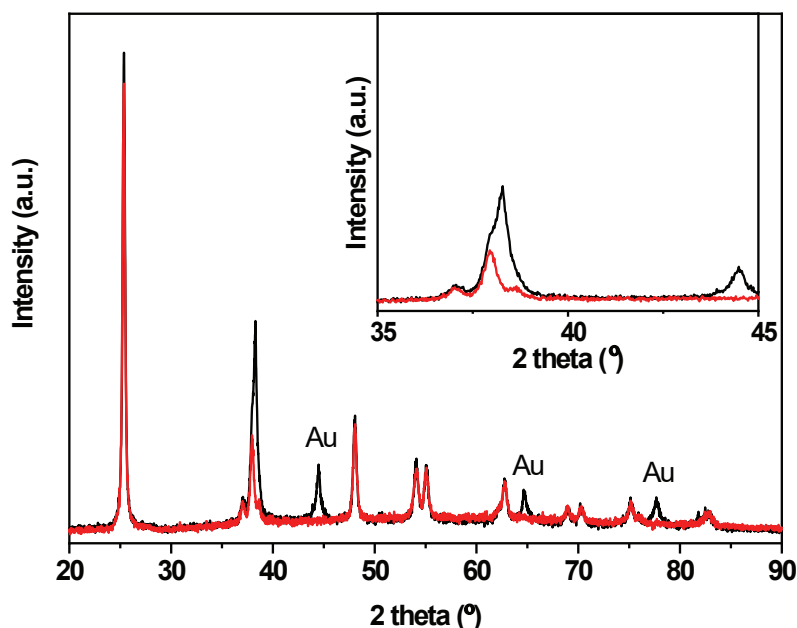

Figure 2. XRD spectra of TiO$_2$ nanotubes and TiO$_2$Au catalyst (2.6 wt% Au). Peaks overlapping are shown as an inset.

TiO$_2$ nanotubes anatase phase and gold phase (Dai et al. 2008)

Raman Spectroscopy was also used to complete the understanding of the material obtained. The sample bands at 144 (Eg), 399 (B1g), 515 (B1g) + (A1g) and 197/639 (Eg) cm^{-1} are shown in Fig. 3b. According to the literature available, it is basically the anatase spectrum (tetragonal anatase, D$_{4h}$ symmetry group). The three samples, which differ only with respect to Au loading, were also analyzed by Raman (Fig. 3a). The set presented no changes in the vibration modes of TiO$_2$, suggesting maintenance of its crystalline phase after the synthesis procedure, validating XRD data presented before. The peak observed close to 144 cm^{-1}, relative to anatase phase of

TiO$_2$ of a single crystal, is progressively enlarged and its Raman maximum peak position is shifted to higher wavenumbers as Au loading increases, indicating augmentation of local crystalline defects within TiO$_2$ lattice structure (contact regions with Au) (Li et al. 2007) Such defects can influence the characteristic anatase vibrational frequency and improve the catalysis process as a whole since they act as photoelectron traps (Zhao & Yang 2016). Therefore, both the X-ray diffraction and Raman spectroscopy analyzes agree that the treatment at 400°C crystallized the TiO$_2$ nanotubular matrix into a major anatase phase. In addition, in the TiO$_2$Au samples, both techniques showed that the Au immobilization affects some structural and surface properties of TiO$_2$, suggesting a good interfacial interaction between the TiO$_2$ semiconductor and the SPR band of the Au NPs.

Diffuse reflectance spectra of bare TiO$_2$ NTs and of Au decorated TiO$_2$ NTs are shown in Fig. 4. It is possible to observe the TiO$_2$ bandgap transition, with a maximum in the UV region (blue line), and the Au SPR band in the visible region (red line). The position and shape of the SPR depend on the particle size, shape and dielectric constant of the medium (Kelly et al. 2003); in our case, the plasmon absorption occurs at 550 nm, resulting in an absorption enhancement in the visible region in the TiO$_2$Au sample (2.6 wt% Au). Basically, the photocatalytic performance of the catalyst is affected by the metal loading of the semiconductor, as shown in Fig. 5. The UV analysis showed characteristic plasmon resonance peaks centered 550 nm for colloidal Gold. As discussed earlier, the SPR is affected by several parameters such as size, morphology, the composition of the nanoparticles and dielectric properties of the surrounding medium. The dielectric constant of TiO$_2$ is estimated to be 42; Au NPs embedded in TiO$_2$ without linkers prompt a strong coupling between Au NPs and TiO$_2$, that
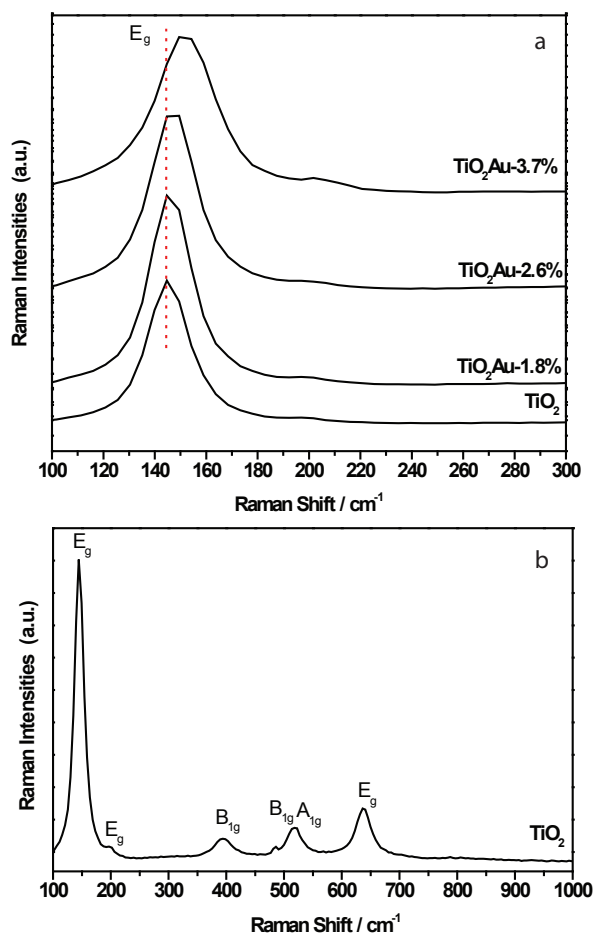

Figure 3. Raman spectra of (a) pure TiO$_2$ and (b) TiO$_2$Au with different Au loadings.
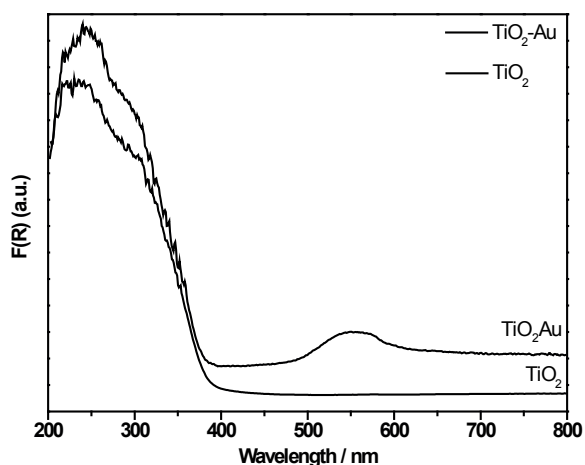
Figure 4. Diffuse reflectance UV-visible spectra of bare TiO$_2$ nanotubes and of Au (2.6 wt%) decorated TiO$_2$ nanotubes.

leads to a large redshift of the SPR absorption band of Au nanoparticles to 550 nm with a slight increase of absorption intensity of TiO$_2$ in the UV-visible region. The slight increase of intensity can also be the result of charge transfer from Ti^{+3} to the oxygen anion of the TiO$_6$ complex.

Table I Shows that the H$_2$ evolution is higher for all the TiO$_2$Au samples when they are compared to the bare TiO$_2$ NTs (under UV-Vis radiation). The better performance was observed for the 2.6 wt% Au sample, which presented an improvement of 760% on the H$_2$ photogeneration in comparison to the bare TiO$_2$ NTs. These results are superior when compared to catalysts synthesized from another way present in the literature (Feil et al. 2010, Xinhua et al. 2018). From there, we characterize and use only the catalyst with 2.6% Au due to high activity.

As expected, the deposition of AuNPs on to the nanotubes surface can facilitate the electrons capture, responsible for the reduction reaction giving rise to molecules of H$_2$ (Fujishima et al. 2008). The Au NPs enhanced the efficiency of photocatalyst mainly by two mechanisms, as proposed in Fig. 5. When the samples are

irradiated with visible light, the electrons are generated on the Au by SPR effect and transferred to the TiO$_2$ NTs, which contribute to the redox reaction for the H$_2$ evolution (Fig. 5a) (Patra & Gopinath 2016, Xinhua et al. 2018). When the samples are irradiated with UV radiation, the electron-hole pairs are generated on the TiO$_2$ and the electrons are transfer to the Au co-catalyst surface, diminishing the recombination, with a more efficient charge separation. This electron transfer is possible since the Fermi energy level for Au is lower than the TiO$_2$ NTs (Fig. 5b).

In general, metal cocatalysts present large work functions that result in robust Schottky barriers effects and, consequently, better charge separations (Warren & Thimsen 2012). On the other hand, when the Au loading increase to 3.7 wt%, the efficiency of the system decrease when compared to the 2.6 wt% Au sample. This effect occurred due to an excess of NPs on the surface of the NTs, inhibiting the photogeneration of electrons on the surface, since such excess acted as a "shield", blocking part of the incident photons, avoiding them to interact with the semiconductor surface. Another effect of an excess of NPs is a mass transport declination, ending up in a reaction rate decreasing as the NPs may act as points of charge recombination (Murdoch et al. 2011).

For a better understanding of the effect on the UV and visible irradiations role, H$_2$ evolution experiments were carried out using different filters. The H$_2$ evolution versus time for UV and visible irradiations are shown in Fig. 6 for pure TiO$_2$ and samples with 0, 1.8, 2.6 and 3.7 wt% Au content. Under UV irradiation, the Au samples have similar effects on the TiO$_2$ photocatalytic efficiency, reaching 11% of augmentation when compared to the sample without gold, in 3 h of reaction. This improvement is related to the better charge separation when the Au NPs are present on the TiO$_2$ surface due to the synergetic
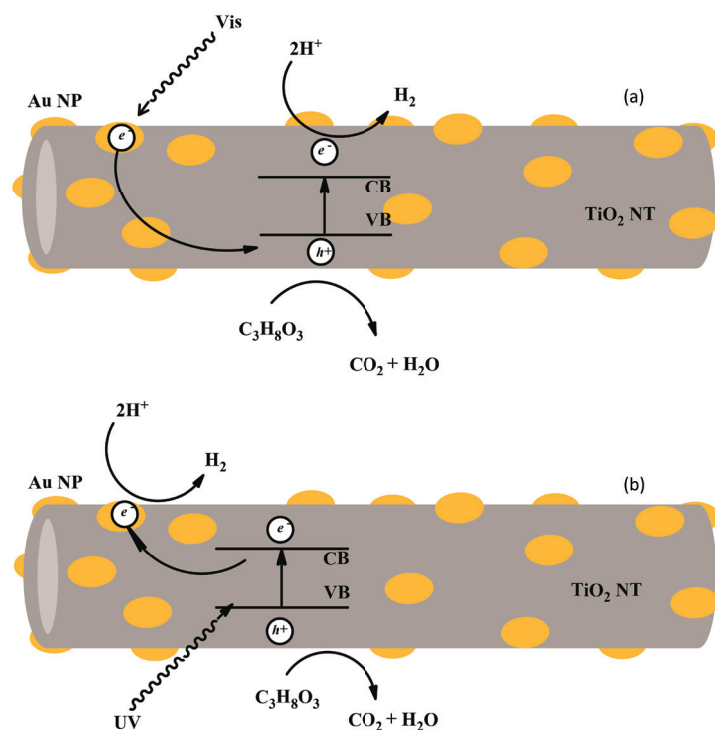
Figure 5. Schematic illustration of TiO$_2$ modified NPs mechanism of under Vis (a) and (b) UV light irradiation.

effect discussed before. On the other hand, when the system was irradiated with visible light only, the H$_2$ evolution had a great improvement for TiO$_2$ NTs (inactive with visible light) with 2.6 wt% Au content. This enhancement under visible irradiation is related to the better absorption in this region due to the plasmonic resonance of Au NPs. The electrons generated in the Au NPs are transferred to TiO$_2$ due to the good interface between the substances and participate in the redox reaction for H$_2$ generation. The excellent interface is formed during the synthesis process, which was performed without molecular ligands. Such molecules can act as interferences for electron transfer in similar TiO$_2$-Au systems (Ding et al. 2014). For sample with 3.7% Au content , we observed a decrease in photocatalytic activity due to photocatalyst surface passivation (Enachi et al. 2015).

Figure 7 Shows the cycle graph for the sample with 2.6 wt% Au. The experiments were conducted at a regular time interval of 5 h illumination and subsequent evacuation of

the evolved gases. In all cycles the generation profile is maintained with average H$_2$ production of 540.31 µmol.g^{-1}. This confirms the excellent stability of the proposed system due to decrease in the rate of recombination of the system.(Jiang et al. 2008) This stability is promoted by the easy charge transfer caused by the exceptional distribution of Au nanoparticles in the surface of the nanotubes obtained without the addition of binders.

CONCLUSIONS

We have performed a systematic study on the synthesis and catalytic activity of TiO$_2$ NTs decored with Au NPs with different metal content for photogeneration of H$_2$. The synthesis approach used herein allowed a facile preparation of Au NPs with similar sizes (12 nm), no matter which metal loading was chosen, without the use of molecular capping ligands. This strategy enhanced the formation of interfaces between the Au NPs and TiO$_2$ NTs. Such improved

Table I. Photogeneration of H$_2$ in 3 h of reaction with TiO$_2$Au materials with variations of Au loading (under UV-Vis radiation).

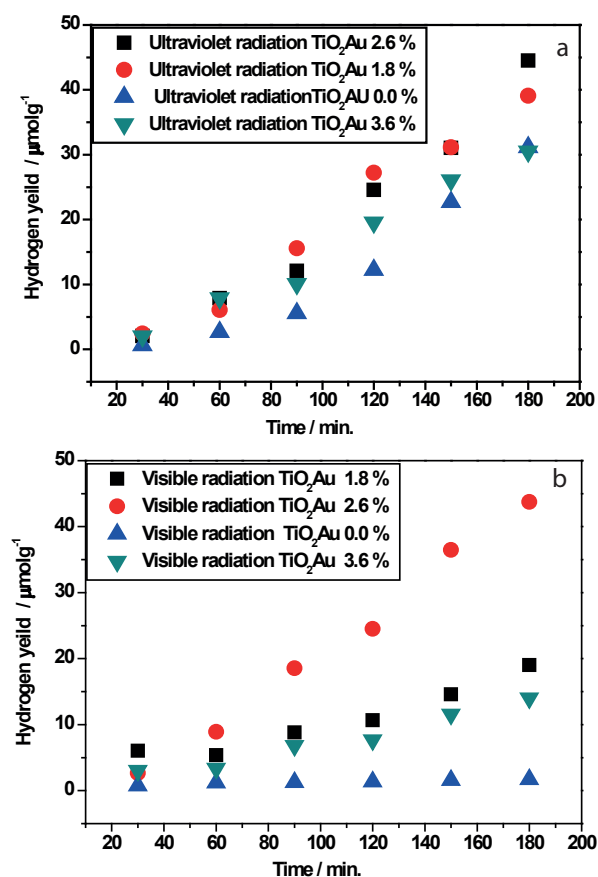| Catalyst	TiO$_2$	TiO$_2$Au	TiO$_2$Au	TiO$_2$Au
Au Concentration	0.0 %	1.8 %	2.6 %	3.7 %
Hydrogen yeld μmolg^{-1}	28	90.4	212.3	88.1

Figure 6. Photogeneration evolution of H$_2$ under (a) ultraviolet and (b) visible irradiation using TiO$_2$Au with 0.0, 1.8, 2.6 and 3.7 wt% Au.

interfaces allowed the Au NPs act as cocatalysts and enhance the H$_2$ generation for the TiO$_2$-based materials by using both UV and visible light irradiations. Under UV irradiation, the Au
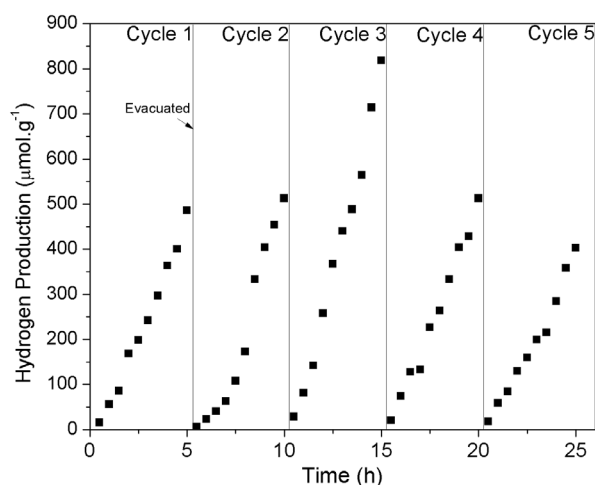

Figure 7. Hydrogen generation under UV-Vis irradiation, during five successive cycles of 5h.

NPs acted in improving the charge separation efficiency, diminishing the charge recombination in the TiO$_2$ semiconductor. However, under visible light, the Au NPs absorbed in this region by plasmonic resonance and the electrons were transferred to the TiO$_2$ and participated in the redox reaction for H$_2$ generation, remarkably increasing the photocatalytic efficiency of the hybrid catalysts.

Acknowledgments

Technology of the Northeast (CETENE-PE). The authors declare that there is no conflict of interest regarding the publication of this paper.

REFERENCES

BAMWENDA GR, TSUBOTA S, NAKAMURA T & HARUTA M. 1995. Photoassisted hydrogen production from a water-ethanol solution: a comparison of activities of AuTiO2 and PtTiO2. J Photochem Photobiol A Chem 89: 177-189.

BESSARABOV D, WANG H, LI H & ZHAO N 2016. PEM Electrolysis for Hydrogen Production: Principles and Applications. CRC Press.

CHO IS, CHOI J, ZHANG K, KIM SJ, JEONG MJ, CAI L, PARK T, ZHENG X & PARK JH. 2015. Highly Efficient Solar Water Splitting from Transferred TiO2 Nanotube Arrays. Nano Lett 15: 5709-5715.

DAI W, CHEN X, WANG X, LIU P, LI D, LI G & FU X. 2008. CO Preferential oxidation promoted by UV irradiation in the presence of H2 over Au/TiO2. Phys Chem Chem Phys 10: 3256-3262.

DING D, LIU K, HE S, GAO C & YIN Y. 2014. Ligand-Exchange Assisted Formation of Au/TiO2 Schottky Contact for Visible-Light Photocatalysis. Nano Lett 14: 6731-6736.

ENACHI M, GUIX M, BRANISTE T, POSTOLACHE V, CIOBANU V, URSAKI V, SCHMIDT OG & TIGINYANU I. 2015. Photocatalytic properties of TiO2 nanotubes doped with Ag, Au and Pt or covered by Ag, Au and Pt nanodots. Surf Eng App Electrochem 51: 3-8.

FEIL AF ET AL. 2010. Growth of TiO2 nanotube arrays with simultaneous Au nanoparticles impregnation: photocatalysts for hydrogen production. J Braz Chem Soc 21: 1359-1365.

FUJISHIMA A & HONDA K. 1972. Electrochemical Photolysis of Water at a Semiconductor Elect. Nat 238: 37-38.

FUJISHIMA A, ZHANG X & TRYK DA. 2008. TiO2 photocatalysis and related surface phenomena. Surface Sci Rep 63: 515-582.

GAO Y, FAN X-B, ZHANG W-F, ZHAO Q-S, ZHANG G-L, ZHANG F-B & LI Y. 2014. Enhanced photocatalytic degradation of methyl orange by Au/TiO2 nanotubes. Mater Lett 130: 1-4.

GOMES SILVA C, JUÁREZ R, MARINO T, MOLINARI R & GARCÍA H. 2011. Influence of Excitation Wavelength (UV or Visible Light) on the Photocatalytic Activity of Titania Containing Gold Nanoparticles for the Generation of Hydrogen or Oxygen from Water. J Am Chem Soc 133: 595-602.

HOFFMANN MR, MARTIN ST, CHOI W & BAHNEMANN DW. 1995. Environ Appl Semi Photoc. Chem Rev 95: 69-96.

JIANG J, GAO Q & CHEN Z. 2008. Gold nanocatalysts supported on protonic titanate nanotubes and titania nanocrystals. J Mol Catal A: Chem 280: 233-239.

KELLY KL, CORONADO E, ZHAO LL & SCHATZ GC. 2003. The Optical Properties of Metal Nanoparticles: The Influence of Size, Shape, and Dielectric Environment. J Phys Chem B 107: 668-677.

KONGKANAND A, TVRDY K, TAKECHI K, KUNO M & KAMAT PV. 2008. Quantum Dot Solar Cells. Tuning Photoresponse through Size and Shape Control of CdSe–TiO2 Architecture. J Am Chem Soc 130: 4007-4015.

LEE K, HAHN R, ALTOMARE M, SELLI E & SCHMUKI P. 2013. Intrinsic Au Decoration of Growing TiO2 Nanotubes and Formation of a High-Efficiency Photocatalyst for H2 Production. Adv Mat 25: 6133-6137.

LI H, BIAN Z, ZHU J, HUO Y, LI H & LU Y. 2007. Mesoporous Au/TiO2 Nanocomposites with Enhanced Photocatalytic Activity. J Am Chem Soc 129: 4538-4539.

LIU B & AYDIL ES. 2009. Growth of Oriented Single-Crystalline Rutile TiO2 Nanorods on Transparent Conducting Substrates for Dye-Sensitized Solar Cells. J Am Chem Soc 131: 3985-3990.

LIU L, OUYANG S & YE J. 2013. Gold-Nanorod-Photosensitized Titanium Dioxide with Wide-Range Visible-Light Harvesting Based on Localized Surface Plasmon Resonance. Angewandte Chem Int Ed 52: 6689-6693.

LOPEZ-SANCHEZ JA ET AL. 2011. Facile removal of stabilizer-ligands from supported gold nanoparticles. Nat Chem 3: 551-556.

MILLSTONE JE, HURST SJ, MÉTRAUX GS, CUTLER JI & MIRKIN CA. 2009. Colloidal Gold and Silver Triangular Nanoprisms. Small 5: 646-664.

MURDOCH M, WATERHOUSE GIN, NADEEM MA, METSON JB, KEANE MA, HOWE RF, LLORCA J & IDRISS H. 2011. The effect of gold loading and particle size on photocatalytic hydrogen production from ethanol over Au/TiO2 nanoparticles. Nat Chem 3: 489.

NI M, LEUNG MKH, LEUNG DYC & SUMATHY K. 2007. A review and recent developments in photocatalytic water-splitting using TiO2 for hydrogen production. Renew Sust Energ Rev 11: 401-425.

PATRA K & GOPINATH C. 2016. Bimetallic and Plasmonic Ag-Au on TiO 2 for Solar Water Splitting: An Active Nanocomposite for Entire Visible-Light-Region Absorption. ChemCatChem 8.

REICHERT R, JUSYS Z AND BEHM RJ. 2015. Au/TiO2 Photo(electro)catalysis: The Role of the Au Cocatalyst in Photoelectrochemical Water Splitting and Photocatalytic H2 Evolution. J Phys Chem C 119: 24750-24759.

RYCENGA M, COBLEY CM, ZENG J, LI W, MORAN CH, ZHANG Q, QIN D & XIA Y. 2011. Controlling the Synthesis and Assembly of Silver Nanostructures for Plasmonic Appl. Chem Rev 111: 3669-3712.

SCHWENGBER CA, ALVES HJ, SCHAFFNER RA, DA SILVA FA, SEQUINEL R, BACH VR & FERRACIN RJ. 2016. Overview of glycerol reforming for hydrogen production. Renew Sust Energ Rev 58: 259-266.

VAIDYA PD & RODRIGUES AE. 2009. Glycerol Reforming for Hydrogen Production: Rev Chem Eng Technol 32: 1463-1469.

WARREN SC & THIMSEN E. 2012. Plasmonic solar water splitting. Energy Environ Sci 5: 5133-5146.

XINHUA DU YL, HUI I & QUANJUN XIANG. 2018. Preparation of Au/TiO$_2$/MoS$_2$ Plasmonic Composite Photocatalysts with Enhanced Photocatalytic Hydrogen Generation Activity. Acta Physico-Chimica Sinica 34: 414-423.

YOUNG JL, STEINER MA, DÖSCHER H, FRANCE RM, TURNER JA & DEUTSCH TODD G. 2017. Direct solar-to-hydrogen conversion via inverted metamorphic multi-junction semiconductor architectures. Natu Energy 2: 17028.

ZHANG J, WANG T, LIU P, LIAO Z, LIU S, ZHUANG X, CHEN M, ZSCHECH E & FENG X. 2017. Efficient hydrogen production on MoNi(4) electrocatalysts with fast water dissociation kinetics. Nat Commun 8: 15437.

ZHAO D & YANG C-F. 2016. Recent advances in the TiO2/CdS nanocomposite used for photocatalytic hydrogen production and quantum-dot-sensitized solar cells. Renew Sustain Energy Rev 54: 1048-1059.

SUPPLEMENTARY MATERIAL

Figure S1. Histogram distribution of TiO$_2$. nanotubes.
Figure S2. Histogram particle size distribution of Au nanoparticles loaded TiO$_2$ nanotubes.
Figure S3. EDS analysis of TiO2Au with 1.8 wt% Au.

JEAN CLAUDIO S. COSTA[1]
https://orcid.org/0000-0002-3037-2329

NOELIA FRANCO[2]
https://orcid.org/0000-0002-1017-2450

THIAGO ANDRÉ S. SOARES[2]
https://orcid.org/0000-0001-6383-5476

NAYTHALLA ANGELA M. SARAIVA[1]
https://orcid.org/0000-0002-4738-9004

MARCO AURÉLIO S. GARCIA[1]
https://orcid.org/0000-0003-3290-9297

JOHAN RENE GONZALEZ[2]
https://orcid.org/0000-0001-6387-1610

GIOVANNA MACHADO[2]
https://orcid.org/0000-0002-9058-3056

[1]Universidade Federal do Piauí, Departamento de Química, Avenida Universitária, s/n, Ininga, 64049-550 Teresina, PI, Brazil

[2]Centro de Tecnologias Estratégicas do Nordeste, Av. Prof. Luís Freire, 1, Cidade Universitária, 50740-545 Recife, PE, Brazil

Correspondence to: **Jean Claudio Santos Costa**
E-mail: jean-cla@ufpi.edu.br

Author contributions

The manuscript was written through the contribution of all authors, specifically: conceptualization, J.C.S.C and G.M; methodology, J.C.S.C, N.F and G.M..; investigation, J.C.S.C., N.F., N.A.N.S., J.R.G.,M.A.S.G. and G.M.; resources, J.C.S.C. and G.M supervision, J.C.S.C. and G.M.; project administration, J.C.S.C. and G.M.; funding acquisition, J.C.S.C. and G.M. All authors have given their approval to the final version of the manuscript.